

# Moderate bending strain induced semiconductor to metal transition in Si nanowires

M. Golam Rabbani<sup>1</sup>, Sunil R. Patil<sup>2</sup>, M. P. Anantram<sup>1</sup>

<sup>1</sup>Department of Electrical Engineering, University of Washington, Seattle, WA 98195 USA, <sup>2</sup>Department of Physics, College of Engineering, Pune, 411005 MS, India

## Abstract

Moderate amount of bending strains, ~3% are enough to induce the semiconductor-metal transition in Si nanowires of ~4nm diameter. The influence of bending on silicon nanowires of 1 nm to 4.3 nm diameter is investigated using molecular dynamics and quantum transport simulations. Local strains in nanowires are analyzed along with the effect of bending strain and nanowire diameter on electronic transport and the transmission energy gap. Interestingly, relatively wider nanowires are found to undergo semiconductor-metal transition at relatively lower bending strains. The effect of bending strain on electronic properties is then compared with the conventional way of straining, i.e. uniaxial, which shows that, the bending is much more efficient way of straining to enhance the electronic transport and also to induce the semiconductor-metal transition in experimentally realizable Si nanowires.

## 1. Introduction

Silicon nanowires (SiNWs) have been employed in numerous electronic devices (e.g. nanotransistors [1]–[3], solar cells [4]–[6]), optoelectronic devices [7], sensors [8]–[11], as well as thermoelectric energy conversions [12], [13]. They can be fabricated/synthesized in both top-down and bottom-up approaches, with a wide range of diameters; from a few nanometers to a few

hundred nanometers. The sub-10 nm diameter nanowires are particularly interesting, as, unlike the bulk silicon and the wider wires, they can have a direct bandgap [14]–[16]. More interestingly, the bandgap of the narrow SiNW can be efficiently strain engineered [14], [17] to an extent of strain induced reversible direct to indirect bandgap transition [14], [15] and also semiconductor to metal transition [18]. This opens up the possibility and realizations of strain modulated not only electronic but also optoelectronic properties of SiNWs.

The traditional objective of straining semiconductor devices is to enhance their mobility through lattice mismatch and stress-memorization [19] [20]–[22] techniques. For NWs though, bending of a substrate containing the nanowires [23], [24] or deposition of an extra layer of straining materials [25], such as oxide, nitride and carbide [18], on a part or the entire length of the wire are more common. Bottom up synthesized nanowires are also unintentionally [26], [27] or intentionally [28], strained and are found to be stable up to over 40% bending strain [29] and a U-shape bending [30]. In fact it is noted that, as nanowire diameter decreases, the bending strength increases [30]. These studies [29] [30], indicate that narrow SiNWs, in addition to demonstrating quantum mechanical properties, also offer mechanical stability under large stresses.

When it comes to model and simulate the strain effect on electronic properties, there have been numerous attempts, which are usually carried out at the density functional theory (DFT) and classical molecular dynamics (MD) level [17], [31]. However, owing to computationally expensive nature of DFT, the device size is usually limited to few 100s of atoms. Often, the finite size effect is countered by using periodic boundary condition (PBC). Most of the investigations, in this field are therefore limited to uniformly strained material systems. This is largely due to non-uniform strain such as bending does not preserve the crystal symmetry, without which PBC cannot be applied along the length of the nanowire. Alternatively, one may consider long enough NWs,

which however, increases the computational demand to the unmanageable level. MD can handle larger system sizes and therefore, is widely used in the study of mechanical [32], [33] and thermal [34], [35] properties of microscale- [36] and nanoscale-devices [37], [38], including silicon nanowires [35], [39]–[50]. However, only reference [50] have studied the effect of bending on electronic properties of nanowires. On the experimental front, it is understood that bending of NWs increases the conductivity in Si as well as in ZnO and CdS [51], [52]. It is to be noted that bending is not limited to only bottom up nanowires, top-down fabricated nanowires can also be bent intentionally [53], [54] or unintentionally [55], [56]. Moreover, top down and bottom up approaches can be combined [57] to get horizontally suspended, well-oriented and size-controlled nanowire arrays. These bending approaches may open up new possibilities, and thus, further investigations on bent nanowires have become crucial.

Therefore, this work investigates the effect of bending on electronic properties of SiNWs. Particularly, the approach involves bent SiNWs optimized with MD, whose output, i.e. atomic coordinates are fed to tight binding model to obtain the electronic Hamiltonian. With this Hamiltonian we perform the quantum transport calculation within the non-equilibrium Green's function [58] formulation. We also present the comparative results of bent nanowires with that of the uniaxially strained nanowires. The paper is organized as follows, the section 2 describes the simulation methodology followed by section 3, which includes strain analysis, results and discussion on the effect of bending on electronic properties of NWs, and the section 4 concludes the work with the conclusion section.

## **2. Methodology**

Six different cross-sectional area,  $\langle 110 \rangle$  directed SiNWs are studied, as sub-10nm diameter nanowires grow mainly along the  $\langle 110 \rangle$  direction [27], [59]–[63]. The average diameters of the nanowires are 1.0 nm, 1.7 nm, 2.3 nm, 3.1 nm, 3.6 nm and 4.3 nm, which are labeled here as  $\langle 110 \rangle 2d$ ,  $\langle 110 \rangle 3d$ ,  $\langle 110 \rangle 4d$ ,  $\langle 110 \rangle 5d$ ,  $\langle 110 \rangle 6d$  and  $\langle 110 \rangle 7d$ , respectively. The total length of each nanowire is 19.922 nm with 103 atomic layers. The initial nanowire structures were generated by the repetition of DFT optimized silicon unit cells [14]. The MD is performed with the Large-scale Atomic/Molecular Massively Parallel Simulator (LAMMPS) [64]. The Tersoff [65], [66] many-body bond-order reactive potential is used to describe the Si-Si interactions. The nanowire structure is first optimized by using energy minimization, with no velocity or force restrictions on any atoms. We follow bending procedure, which was used for bending the silicon carbide nanowires [32], where the Si atoms are subdivided into three groups. To apply bending stress to the middle group, the atoms in the left (right) group are rotated counter clockwise (clockwise) in the yz plane (Supplementary Information Figure 1(b) top) by an angle of 0.05 degree. Then they are kept frozen while energy minimization is done to the middle group of atoms. After the minimization, the atomic positions of all the atoms are saved, and the process is repeated for the next increment of the rotation angle. Similar approach is used for uniaxial strain, by shifting the end atoms, instead of rotating them. Since the left and right groups of atoms are kept fixed during the bending or uniaxial straining and energy minimization process, the atoms in the middle group, which are close to atoms in the edge groups, undergo artificial deformations. To avoid this, 19 layers of atoms from each end are cropped off. Next, the remaining 65 layers are hydrogen passivated with the GaussView [67], and then were used for tight binding and quantum transport calculations. We employ the  $sp^3d^5s^*$  tight binding (TB) method with parameters from Jancu [68] to form electronic Hamiltonian matrix. Without considering spin-orbit coupling in  $sp^3d^5s^*$  TB,

Hamiltonian size for each silicon atom is  $10 \times 10$ , and that for each hydrogen atom is  $1 \times 1$ . Thus, the Hamiltonian size of each layer is between  $128 \times 128$  ( $\langle 110 \rangle 2d$ ) and  $1498 \times 1498$  ( $\langle 110 \rangle 7d$ ). The Hamiltonian formed by TB is used to calculate the transmission through the nanowire by using the non-equilibrium Green's function (NEGF)[58] formalism. For ballistic transport, the electronic transmission in a semiconductor is zero in the energy bandgap, therefore, transmission can be used to estimate the energy bandgap.

### 3. Results and Discussion

#### 3.1 Strain analysis

In this subsection, we analyze the strains in the nanowires. Figure 1 shows three bent nanowires, (a)  $\langle 110 \rangle 3d$ , (b)  $\langle 110 \rangle 5d$ , and (c)  $\langle 110 \rangle 7d$ , with their local atomic strain along the length ( $z$ ) direction visualized as color variation. To obtain this strain configuration, the left and right atom groups of each nanowire was rotated by  $15^\circ$  in the vertical ( $yz$ ) plane. The top side of each nanowire is under tension while the bottom side is under compression. The corner atoms are under the largest amount of strain due to the rotation. Also for a fixed amount of rotation, as expected, the range of strain variation (from most compressive to most tensile) increases with the nanowire diameter. In addition, the largest tensile strain magnitude is always higher than the largest compressive strain magnitude, for example,  $+3.7\%$  vs  $-2.3\%$  for nanowire  $\langle 110 \rangle 3d$ . This is due to the atomic potentials resisting compression more than tension because as the atoms are brought closer to each other beyond the no-strain minimum energy position the energy increases exponentially.

Figure 2, therefore, plots all the three strain ranges ( $x$ -range (a),  $y$ -range (b), and  $z$ -range (c)) as a function of the nanowire diameter for different amount of end-atom-group rotations. The

ranges are almost linearly proportion to the nanowire diameter. The y-range values are slightly higher than the x-range values as diameter along y is wider. Due to bending along the length, z-range values are the largest.

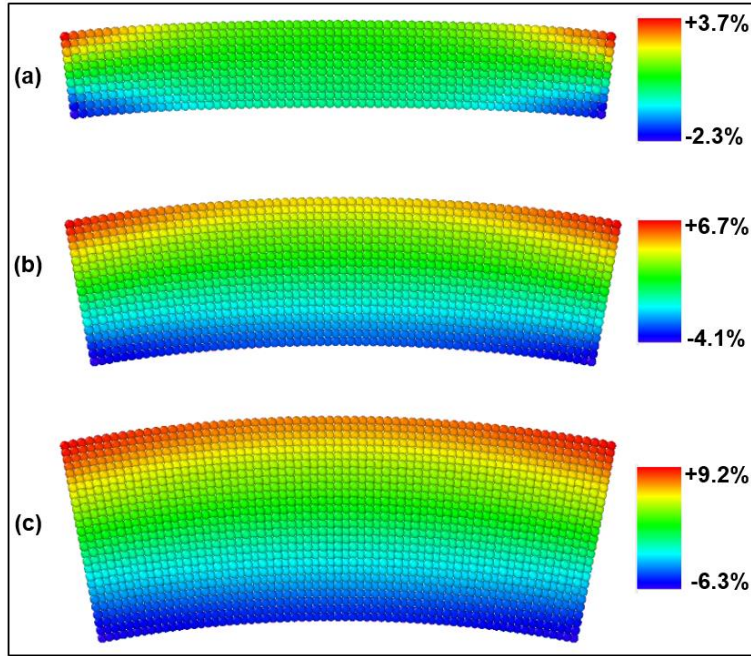


Figure 1. Local strain along the **z-direction (length)** in 3 different nanowires as a color plot; (a)  $\langle 110 \rangle 3d$ , (b)  $\langle 110 \rangle 5d$ , (c)  $\langle 110 \rangle 7d$ .

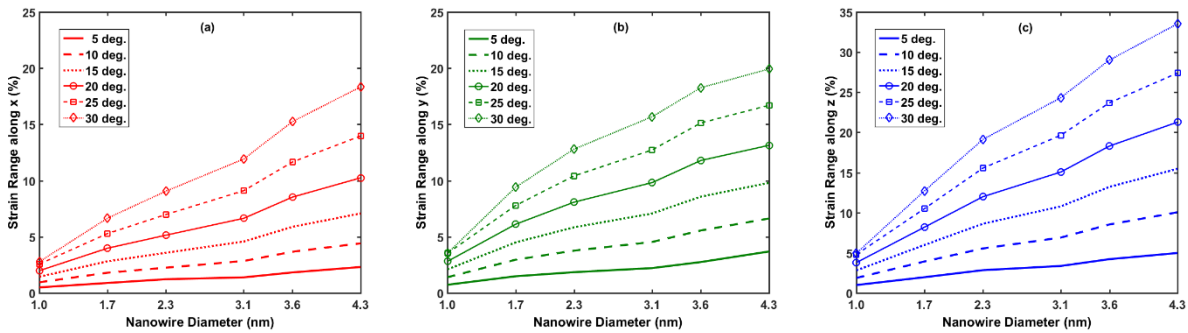


Figure 2. Ranges of strain (x-range (a), y-range (b) and z-range (c)) as functions of nanowire diameter for different amount of end-atom-group rotations. x and y directions are in the cross-sectional plane while z is along the length. x dimension is smaller than y dimension. For each case, bottom curve is for smallest rotation (5 deg.) and the rotation increases upwards.

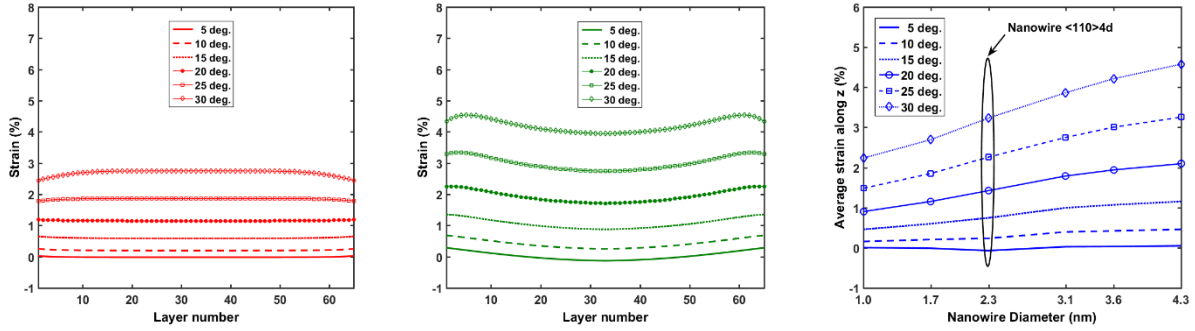


Figure 3. Layer to layer average strain along length: (a)  $\langle 110 \rangle 3d$ , and (b)  $\langle 110 \rangle 6d$ . (c) Average strain along length as a function of diameter for all six nanowires. Nanowire  $\langle 110 \rangle 4d$  has been pointed out.

Figure 3(a) and b) plots the layer to layer strain along the length, as defined in equation (1), for two different nanowires - (a)  $\langle 110 \rangle 3d$  and (b)  $\langle 110 \rangle 6d$ . We have already seen in Figure 2(c) that the range of variation of  $z$ -strain over all the atoms in a nanowire can be quite large, mainly because of the corner atoms being under large strain of opposite polarity. However, the layer to layer strain variation is actually smaller (Figure 3(a) and (b)). As variation is small, it is possible to find a single quantity, representing an equivalent average strain, for each of the curves in Figure 3. This average number is plotted in Figure 3(c) for all the bent nanowires considered in this study. For the same end-atom rotation, the average strain increases linearly with the diameter, like the strain ranges. The average strain value is used for studying correlation with electronic properties and comparison with uniaxially strained nanowires, for which nominal strain value along length is used.

### 3.2 Electronic transmission

In bent nanowires, the bending strain compresses or extends the nanowire locally (Figure 1), although on an average, the nanowire is under tensile strain along the length (Figure 3(c)). The

strain (bending or uniaxial) changes the electronic band profile of the nanowire [69]. Due to the absence of crystal symmetry under bending, one cannot determine the energy band structure using the Bloch's theorem. We rather calculate the electronic transmission (Supplementary Information Eq. (5)) in the strained nanowires as a function of energy, which has information about the energy gap as well as transmission probability.

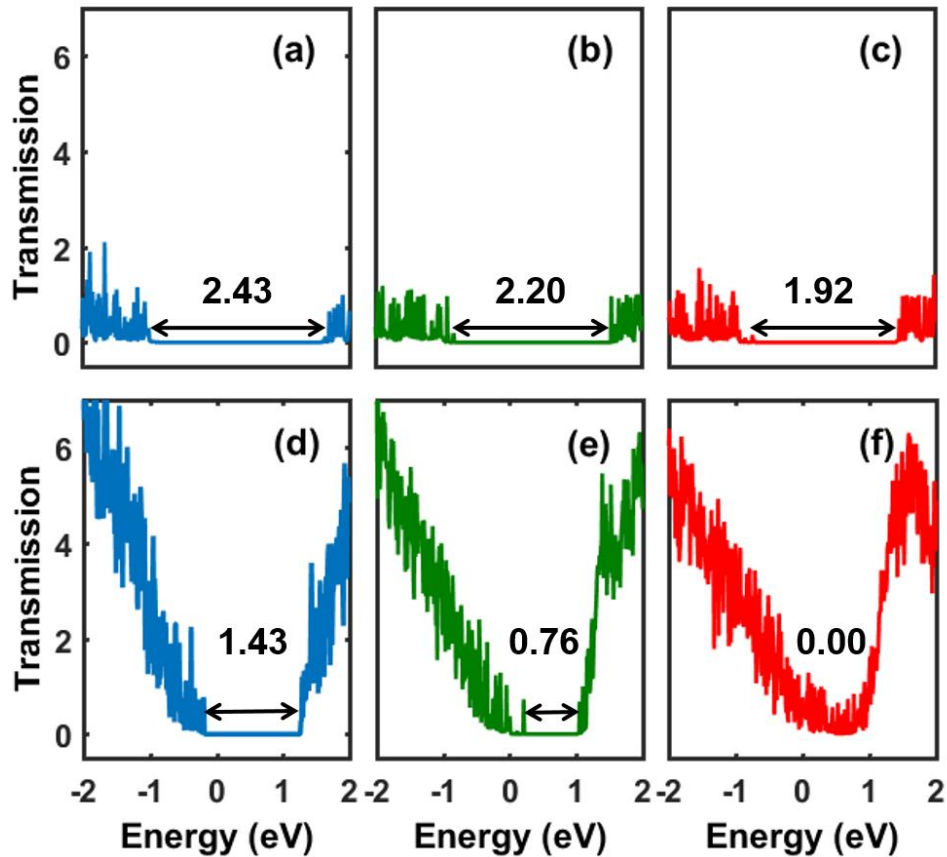


Figure 4. Electronic transmission through two nanowires as a function of energy for different bending angles.

Narrowest  $\langle 110 \rangle 2d$  nanowire with no rotation (a), with 15-degree rotation (b), with 30-degree rotation (c). Widest  $\langle 110 \rangle 7d$  nanowire with no rotation (d), with 15-degree rotation (e), 30-degree rotation (f).

Figure 4 shows the electronic transmission through the nanowires as a function of energy for, respectively, zero, 15-degree and 30-degree end-atom-group rotations: (a, b, c)  $\langle 110 \rangle 2d$  and (d, e, f)  $\langle 110 \rangle 7d$ . We notice three important trends in the plots. First, a narrower nanowire has a lower transmission value. The reason is a narrower nanowire has a fewer number of electronic modes, and, at any energy, transmission is proportional to the number of modes. Second, the transmission gap - the continuous energy range over which the transmission is zero - in the nanowire is larger than the bulk silicon bandgap. As a result of quantum confinement decreasing with increasing NW diameter, the transmission gap decreases as the nanowire diameter increases. The bandgap values, calculated by assuming the entire length of the bent nanowire as a single unit cell, also match with the corresponding transmission gap. In addition, it is to be noticed that the gaps in the unstrained nanowires, 2.43 eV ( $\langle 110 \rangle 2d$ ) and 1.43 eV ( $\langle 110 \rangle 7d$ ), are consistent with those obtained with DFT [14] and DFTB [16]. Third and most importantly, the gap in each nanowire decreases as the amount of bending strain (that is, average strain along length) increases. This behavior is also consistent with the results in [14], which predicts that for an increase in uniaxial tensile strain in the nanowire, its bandgap decreases.

We can get a more comprehensive overview by studying the transmission energy gap as a function of the nanowire diameter with the angle of end atom group rotation as a parameter. Such characteristics are plotted in Figure 5 for no rotation and six different rotations (5, 10, 15, 20, 25, and 30 degree) conditions (solid lines). For small end-atom rotations (top curves), as the nanowire diameter decreases from the largest diameter, 4.3 nm, the gap increases gradually. This increase, however, becomes sharper as the diameter decreases below 1.7 nm. For large rotations, the gap increases almost linearly as the diameter decreases. It is interesting to note that for the two widest wires, diameters 3.6 nm and 4.3 nm, the gap completely disappears for large strains  $\sim 3\%$ , as the

strain range is higher for the wider wires. For large bending, the local strains (both tensile and compression) in some parts of the wider wires are very high (and of opposite direction). These large local strains represent a huge departure from the perfect crystal structure and introduce many electronic modes in the band gap, thereby making the gap totally disappear (Figure 4(f)). This particular phenomena has been reported in relatively thinner core-shell Si-SiC NWs and attributed to the relatively huge compressive strain  $\sim 9\%$  [18]. It has been shown experimentally that bending increases nanowire conductivity [51], [52], so bandgap decrease and conductivity increase can be correlated.

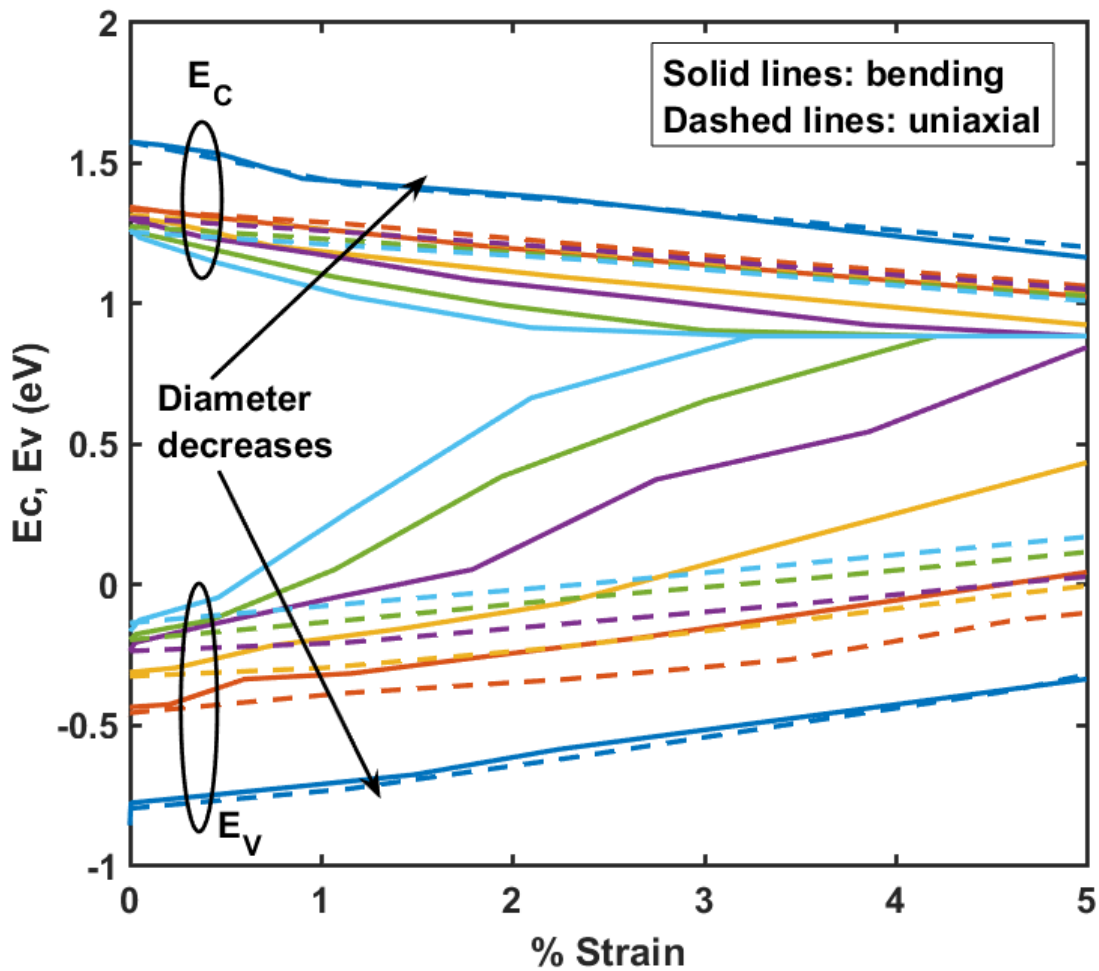


Figure 5.  $E_c$  and  $E_v$  as a function of % strain. Solid: bent, dashed: uniaxial.

### 3.3 Bent nanowire vs. uniaxially strained nanowire

Figure 5 also shows the energy gap in electronic transmission as a function of strain for six nanowires uniaxially strained cases (dashed lines). The gap decreases linearly with the strain for both the method of straining, which agrees with uniaxially strained nanowires studied with DFT [14]. However, for the same diameter and the same average strain, the gap is smaller and its decrease rate is faster in the bent nanowires. The larger decrease rate also means that the strain modulated band gap will respond to wider electromagnetic spectrum. This clearly is an advantage of the bent nanowire over the uniaxially strained nanowire.

It is also to be noted that, for narrow nanowires, both  $E_C$  and  $E_V$  change at a similar rate, but as nanowire diameter increases, the rate of change of  $E_V$  becomes faster, indicating that the bending affects the valence band maxima significantly than that of the conduction band which is also consistent with [18], where similar observations are noted under relatively large compressive strains of ~9%. Similar trends are seen in bi-axially strained silicon and has been attributed to valence band valley splitting in the effective mass approach [69]. It is intricate, which requires additional investigations, to pin point the particular phenomenon leading to the significant upward shift in valence band edge due to the complicated bending strain profile.

We also would like to note here that, although the maximum value of experimentally observed uniaxial strain is about 5% [25], nanowires have been found to withstand large (40%) bending strain [29]. In another study, U-shape bent 40 nm diameter silicon nanowire was stable up to 11.5% strain [30]. So considering the  $E_C$  and  $E_V$  trends vs strain in Figure 5 and the amount of experimentally observed bending strain can be easily achieved experimentally in SiNWs.

## 4. Conclusion

Electronic transport properties SiNWs of diameters from 1 nm to 4.3 nm under bending strain are simulated using MD for structural optimization and NEGF for transport calculations. It is observed that for the same amount of bending, strain range increases with nanowire diameter. The larger strains directly translate into smaller energy gaps in electronic transmission for wider wires. The electronic transport in bent SiNWs are also compared with that of uniaxially strained. Bending is found to be a more efficient way as compared to uniaxial strain, of enhancing the electronic transport and reducing transmission gap, such that SiNWs undergo semiconductor to metal transition at relatively lower strain values. This makes the bending as an efficient straining mechanism over uniaxial in nanowires in respect to conductance enhancements well as modulation of energy gaps to exploit wider electromagnetic spectrum.

## References

- [1] G. Larrieu and X.-L. Han, "Vertical nanowire array-based field effect transistors for ultimate scaling," *Nanoscale*, vol. 5, no. 6, pp. 2437–2441, Mar. 2013.
- [2] J.-P. Colinge, C.-W. Lee, A. Afzalian, N. D. Akhavan, R. Yan, I. Ferain, P. Razavi, B. O'Neill, A. Blake, M. White, A.-M. Kelleher, B. McCarthy, and R. Murphy, "Nanowire transistors without junctions," *Nat. Nanotechnol.*, vol. 5, no. 3, pp. 225–229, Mar. 2010.
- [3] N. Singh, F. Y. Lim, W. W. Fang, S. C. Rustagi, L. K. Bera, a. Agarwal, C. H. Tung, K. M. Hoe, S. R. Omampuliyur, D. Tripathi, a. O. Adeyeye, G. Q. Lo, N. Balasubramanian, and D. L. Kwong, "Ultra-Narrow Silicon Nanowire Gate-All-Around CMOS Devices: Impact of Diameter, Channel-Oriented and Low Temperature on Device Performance," *2006 Int. Electron Devices Meet.*, pp. 1–4, 2006.
- [4] L. Tsakalacos, J. Balch, J. Fronheiser, B. a. Korevaar, O. Sulima, and J. Rand, "Silicon nanowire solar cells," *Appl. Phys. Lett.*, vol. 91, no. 23, p. 233117, 2007.
- [5] M. M. Adachi, M. P. Anantram, and K. S. Karim, "Core-shell silicon nanowire solar cells," *Sci. Rep.*, vol. 3, p. 1546, Jan. 2013.
- [6] E. Garnett and P. Yang, "Light trapping in silicon nanowire solar cells," *Nano Lett.*, vol. 10, no. 3, pp. 1082–1087, Mar. 2010.
- [7] L. Li, C. Yang, H. Junhui, and Y. Qiaowen, "Preparation and Optoelectronic Applications

- of Silicon Nanowire Arrays,” *Prog. Chem. Rev.*, vol. 25, no. 0203, pp. 248–259, 2013.
- [8] Z. Gao, A. Agarwal, A. D. Trigg, N. Singh, C. Fang, C.-H. Tung, Y. Fan, K. D. Buddharaju, and J. Kong, “Silicon nanowire arrays for label-free detection of DNA,” *Anal. Chem.*, vol. 79, no. 9, pp. 3291–7, May 2007.
- [9] G. Zheng, F. Patolsky, Y. Cui, W. U. Wang, and C. M. Lieber, “Multiplexed electrical detection of cancer markers with nanowire sensor arrays,” *Nat. Biotechnol.*, vol. 23, no. 10, pp. 1294–1301, Oct. 2005.
- [10] I. Park, Z. Li, A. P. Pisano, and R. S. Williams, “Top-down fabricated silicon nanowire sensors for real-time chemical detection,” *Nanotechnology*, vol. 21, no. 1, p. 015501, Jan. 2010.
- [11] J. H. Chua, R.-E. Chee, A. Agarwal, S. M. Wong, and G.-J. Zhang, “Label-free electrical detection of cardiac biomarker with complementary metal-oxide semiconductor-compatible silicon nanowire sensor arrays,” *Anal. Chem.*, vol. 81, no. 15, pp. 6266–71, Aug. 2009.
- [12] D. Dávila, a Tarancón, M. Fernández-Regúlez, C. Calaza, M. Salleras, a San Paulo, and L. Fonseca, “Silicon nanowire arrays as thermoelectric material for a power microgenerator,” *J. Micromechanics Microengineering*, vol. 21, no. 10, p. 104007, Oct. 2011.
- [13] a. Stranz, J. Kähler, S. Merzsch, a. Waag, and E. Peiner, “Nanowire silicon as a material for thermoelectric energy conversion,” *Microsyst. Technol.*, vol. 18, no. 7–8, pp. 857–862, Dec. 2011.
- [14] D. Shiri, Y. Kong, A. Buin, and M. P. Anantram, “Strain induced change of bandgap and effective mass in silicon nanowires,” *Appl. Phys. Lett.*, vol. 93, no. 7, p. 073114, 2008.
- [15] X. B. Yang and R. Q. Zhang, “Indirect-to-direct band gap transitions in phosphorus adsorbed <112> silicon nanowires,” *Appl. Phys. Lett.*, vol. 93, no. 17, p. 173108, 2008.
- [16] M. Nolan, S. O’Callaghan, G. Fagas, J. C. Greer, and T. Frauenheim, “Silicon nanowire band gap modification,” *Nano Lett.*, vol. 7, no. 1, pp. 34–8, Jan. 2007.
- [17] D. Shiri, A. Verma, C. R. Selvakumar, and M. P. Anantram, “Reversible modulation of spontaneous emission by strain in silicon nanowires,” *Sci. Rep.*, vol. 2, p. 461, Jan. 2012.
- [18] M. Amato and R. Rurali, “Shell-thickness controlled semiconductor-metal transition in Si-SiC core-shell nanowires,” *Nano Lett.*, vol. 15, no. 5, pp. 3425–3430, 2015.
- [19] S. E. Thompson, M. Armstrong, C. Auth, S. Cea, R. Chau, G. Glass, T. Hoffman, J. Klaus, Z. Ma, B. McIntyre, a. Murthy, B. Obradovic, L. Shifren, S. Sivakumar, S. Tyagi, T. Ghani, K. Mistry, M. Bohr, and Y. El-Mansy, “A Logic Nanotechnology Featuring Strained-Silicon,” *IEEE Electron Device Lett.*, vol. 25, no. 4, pp. 191–193, Apr. 2004.
- [20] C. Ortolland, Y. Okuno, P. Verheyen, C. Kerner, C. Stapelmann, M. Aoulaiche, N. Horiguchi, and T. Hoffmann, “Stress Memorization Technique—Fundamental Understanding and Low-Cost Integration for Advanced CMOS Technology Using a Nonselective Process,” *IEEE Trans. Electron Devices*, vol. 56, no. 8, pp. 1690–1697, Aug.

2009.

- [21] A. Wei, M. Wiatr, A. Mowry, A. Gehring, R. Boschke, C. Scott, J. Hoentschel, S. Duenkel, M. Gerhardt, T. Feudel, M. Lenski, F. Wirbeleit, R. Otterbach, R. Callahan, G. Koerner, N. Krumm, D. Greenlaw, M. Raab, and M. Horstmann, "Multiple Stress Memorization In Advanced SOI CMOS Technologies," in *2007 IEEE Symposium on VLSI Technology*, 2007, pp. 216–217.
- [22] C. Ortolland, P. Morin, C. Chaton, E. Mastromatteo, C. Populaire, S. Orain, F. Leverd, P. Stolk, F. Boeuf, and F. Arnaud, "Stress Memorization Technique ( SMT ) Optimization for 45nm CMOS," vol. 51, no. c, pp. 2005–2006, 2006.
- [23] R. He and P. Yang, "Giant piezoresistance effect in silicon nanowires," *Nat. Nanotechnol.*, vol. 1, no. 1, pp. 42–6, Oct. 2006.
- [24] E. F. Arkan, D. Sacchetto, I. Yildiz, Y. Leblebici, and B. E. Alaca, "Monolithic integration of Si nanowires with metallic electrodes: NEMS resonator and switch applications," *J. Micromechanics Microengineering*, vol. 21, no. 12, p. 125018, Dec. 2011.
- [25] V. Passi, U. Bhaskar, T. Pardoen, U. Södervall, B. Nilsson, G. Petersson, M. Hagberg, and J.-P. Raskin, "High-Throughput On-Chip Large Deformation of Silicon Nanoribbons and Nanowires," *J. MICROELECTROMECHANICAL Syst.*, vol. 21, no. 4, pp. 822–829, 2012.
- [26] S. Hofmann, C. Ducati, R. J. Neill, S. Piscanec, a. C. Ferrari, J. Geng, R. E. Dunin-Borkowski, and J. Robertson, "Gold catalyzed growth of silicon nanowires by plasma enhanced chemical vapor deposition," *J. Appl. Phys.*, vol. 94, no. 9, p. 6005, 2003.
- [27] Y. Cui, L. J. Lauhon, M. S. Gudixsen, J. Wang, and C. M. Lieber, "Diameter-controlled synthesis of single-crystal silicon nanowires," *Appl. Phys. Lett.*, vol. 78, no. 15, p. 2214, 2001.
- [28] W. Molnar, a Lugstein, P. Pongratz, M. Seyring, M. Rettenmayr, C. Borschel, C. Ronning, N. Auner, C. Bauch, and E. Bertagnolli, "A general approach toward shape-controlled synthesis of silicon nanowires.," *Nano Lett.*, vol. 13, no. 1, pp. 21–5, Jan. 2013.
- [29] S. Dai, J. Zhao, L. Xie, Y. Cai, N. Wang, and J. Zhu, "Electron-beam-induced elastic-plastic transition in Si nanowires," *Nano Lett.*, vol. 12, no. 5, pp. 2379–85, May 2012.
- [30] G. Stan, S. Krylyuk, a V Davydov, I. Levin, and R. F. Cook, "Ultimate bending strength of Si nanowires.," *Nano Lett.*, vol. 12, no. 5, pp. 2599–604, May 2012.
- [31] C. Tuma and A. Curioni, "Large scale computer simulations of strain distribution and electron effective masses in silicon  $\langle 100 \rangle$  nanowires," *Appl. Phys. Lett.*, vol. 96, no. 19, p. 193106, 2010.
- [32] M. Makeev, D. Srivastava, and M. Menon, "Silicon carbide nanowires under external loads: An atomistic simulation study," *Phys. Rev. B*, vol. 74, no. 16, p. 165303, Oct. 2006.
- [33] J. Zhang, C. Wang, R. Chowdhury, and S. Adhikari, "Small-scale effect on the mechanical properties of metallic nanotubes," *Appl. Phys. Lett.*, vol. 101, no. 9, p. 093109, 2012.

- [34] P. C. Howell, "Comparison of molecular dynamics methods and interatomic potentials for calculating the thermal conductivity of silicon," *J. Chem. Phys.*, vol. 137, no. 22, p. 224111, Dec. 2012.
- [35] J. Diao, D. Srivastava, and M. Menon, "Molecular dynamics simulations of carbon nanotube/silicon interfacial thermal conductance," *J. Chem. Phys.*, vol. 128, no. 16, p. 164708, Apr. 2008.
- [36] S. Ketten, C.-C. Chou, A. C. T. van Duin, and M. J. Buehler, "Tunable nanomechanics of protein disulfide bonds in redox microenvironments.," *J. Mech. Behav. Biomed. Mater.*, vol. 5, no. 1, pp. 32–40, Jan. 2012.
- [37] Y. Y. Zhang, Q. X. Pei, and C. M. Wang, "Mechanical properties of graphynes under tension: A molecular dynamics study," *Appl. Phys. Lett.*, vol. 101, no. 8, p. 081909, 2012.
- [38] M. Hu and D. Poulikakos, "Si/Ge superlattice nanowires with ultralow thermal conductivity," *Nano Lett.*, vol. 12, no. 11, pp. 5487–94, Nov. 2012.
- [39] Y. He and G. Galli, "Microscopic Origin of the Reduced Thermal Conductivity of Silicon Nanowires," *Phys. Rev. Lett.*, vol. 108, no. 21, p. 215901, May 2012.
- [40] J. Guérolé, J. Godet, and S. Brochard, "Deformation of silicon nanowires studied by molecular dynamics simulations," *Model. Simul. Mater. Sci. Eng.*, vol. 19, no. 7, p. 074003, Oct. 2011.
- [41] Z. Yang, Z. Lu, and Y.-P. Zhao, "Shape effects on the yield stress and deformation of silicon nanowires: A molecular dynamics simulation," *J. Appl. Phys.*, vol. 106, no. 2, p. 023537, 2009.
- [42] K. Kang and W. Cai, "Size and temperature effects on the fracture mechanisms of silicon nanowires: Molecular dynamics simulations," *Int. J. Plast.*, vol. 26, no. 9, pp. 1387–1401, Sep. 2010.
- [43] T. Brun, D. Mercier, a. Koumela, C. Marcoux, and L. Duraffourg, "Silicon nanowire based Pirani sensor for vacuum measurements," *Appl. Phys. Lett.*, vol. 101, no. 18, p. 183506, 2012.
- [44] A. I. Hochbaum, R. Chen, R. D. Delgado, W. Liang, E. C. Garnett, M. Najarian, A. Majumdar, and P. Yang, "Enhanced thermoelectric performance of rough silicon nanowires," *Nature*, vol. 451, no. 7175, pp. 163–7, Jan. 2008.
- [45] A. Agarwal, K. Buddharaju, I. K. Lao, N. Singh, N. Balasubramanian, and D. L. Kwong, "Silicon nanowire sensor array using top–down CMOS technology," *Sensors Actuators A Phys.*, vol. 145–146, pp. 207–213, Jul. 2008.
- [46] T.-M. Chang, C.-C. Weng, and M.-J. Huang, "A Nonequilibrium Molecular Dynamics Study of In-Plane Thermal Conductivity of Silicon Thin Films," *J. Electron. Mater.*, vol. 39, no. 9, pp. 1616–1620, May 2010.
- [47] H. Zhao and N. R. Aluru, "Size and surface orientation effects on thermal expansion coefficient of one-dimensional silicon nanostructures," *J. Appl. Phys.*, vol. 105, no. 10, p. 104309, 2009.

- [48] B. Hong and A. Z. Panagiotopoulos, "Molecular dynamics simulations of silica nanoparticles grafted with poly(ethylene oxide) oligomer chains," *J. Phys. Chem. B*, vol. 116, no. 8, pp. 2385–95, Mar. 2012.
- [49] N. Zhang, Q. Deng, Y. Hong, L. Xiong, S. Li, M. Strasberg, W. Yin, Y. Zou, C. R. Taylor, G. Sawyer, and Y. Chen, "Deformation mechanisms in silicon nanoparticles," *J. Appl. Phys.*, vol. 109, no. 6, p. 063534, 2011.
- [50] I. Ponomareva, M. Menon, D. Srivastava, and A. N. Andriotis, "Structure, Stability, and Quantum Conductivity of Small Diameter Silicon Nanowires," *Phys. Rev. Lett.*, vol. 95, no. 26, p. 265502, Dec. 2005.
- [51] X. Han, G. Jing, X. Zhang, R. Ma, X. Song, J. Xu, Z. Liao, N. Wang, and D. Yu, "Bending-induced conductance increase in individual semiconductor nanowires and nanobelts," *Nano Res.*, vol. 2, no. 7, pp. 553–557, Mar. 2010.
- [52] K. E. Moselund, M. Najmzadeh, S. Member, P. Dobrosz, S. H. Olsen, D. Bouvet, L. De Michielis, V. Pott, A. M. Ionescu, and S. Member, "The High-Mobility Bended n-Channel Silicon Nanowire Transistor," vol. 57, no. 4, pp. 866–876, 2010.
- [53] S. Zhang, L. Lou, and C. Lee, "Piezoresistive silicon nanowire based nanoelectromechanical system cantilever air flow sensor," *Appl. Phys. Lett.*, vol. 100, no. 2, p. 023111, 2012.
- [54] R. Yang, T. He, C. Marcoux, P. Andreucci, L. Duraffourg, P. X. Feng, E. Engineering, C. Western, M. Campus, and G. Cedex, "SILICON NANOWIRE AND CANTILEVER ELECTROMECHANICAL SWITCHES WITH INTEGRATED PIEZORESISTIVE TRANSDUCERS," pp. 1–4, 2013.
- [55] G. Pennelli, M. Totaro, A. Nannini, U. Pisa, V. G. Caruso, and I. Pisa, "Correlation between Surface Stress and Apparent Young ' s Modulus of Top-Down Silicon Nanowires," no. 12, pp. 10727–10734, 2012.
- [56] M. G. Rabbani, "Unpublished," 2011.
- [57] A. S. Paulo, N. Arellano, J. a Plaza, R. He, C. Carraro, R. Maboudian, R. T. Howe, J. Bokor, and P. Yang, "Suspended mechanical structures based on elastic silicon nanowire arrays," *Nano Lett.*, vol. 7, no. 4, pp. 1100–4, Apr. 2007.
- [58] S. Datta, *Electronic Transport in Mesoscopic Systems (Cambridge Studies in Semiconductor Physics and Microelectronic Engineering)*. Cambridge University Press, 1997.
- [59] V. Schmidt, J. V Wittemann, and U. Gösele, "Growth, thermodynamics, and electrical properties of silicon nanowires," *Chem. Rev.*, vol. 110, no. 1, pp. 361–88, Jan. 2010.
- [60] S. M. Eichfeld, M. F. Hainey, H. Shen, C. E. Kendrick, E. A. Fucinato, J. Yim, M. R. Black, and J. M. Redwing, "Vapor-liquid-solid growth of (110) silicon nanowire arrays," in *SPIE NanoScience + Engineering*, 2013, p. 88200I.
- [61] J. V. Wittemann, W. Münchgesang, S. Senz, and V. Schmidt, "Silver catalyzed ultrathin silicon nanowires grown by low-temperature chemical-vapor-deposition," *J. Appl. Phys.*,

- vol. 107, no. 9, p. 096105, May 2010.
- [62] Y. Wu, Y. Cui, L. Huynh, C. J. Barrelet, D. C. Bell, and C. M. Lieber, "Controlled Growth and Structures of Molecular-Scale Silicon Nanowires," *Nano Lett.*, vol. 4, no. 3, pp. 433–436, 2004.
- [63] Z. Huang, T. Shimizu, S. Senz, Z. Zhang, X. Zhang, W. Lee, N. Geyer, and U. Go, "Ordered Arrays of Vertically Aligned [ 110 ] Silicon Nanowires by Suppressing the Crystallographically Preferred <100> Etching Directions 2009," no. 110, 2009.
- [64] S. Plimpton, "Fast Parallel Algorithms for Short – Range Molecular Dynamics," vol. 117, no. June 1994, pp. 1–42, 1995.
- [65] J. Tersoff, "Empirical interatomic potential for silicon with improved elastic properties," *Phys. Rev. B*, vol. 38, no. 14, pp. 9902–9905, Nov. 1988.
- [66] F. de Brito Mota, J. F. Justo, and A. Fazzio, "Hydrogen role on the properties of amorphous silicon nitride," *J. Appl. Phys.*, vol. 86, no. 4, p. 1843, Aug. 1999.
- [67] D. Roy, T. Keith, and J. Millam, "GaussView, Version 5," *Semichem Inc. Shawnee Mission KS*, 2009.
- [68] J.-M. Jancu, R. Scholz, F. Beltram, and F. Bassani, "Empirical sp<sup>3</sup>s\* tight-binding calculation for cubic semiconductors: General method and material parameters," *Phys. Rev. B*, vol. 57, no. 11, pp. 6493–6507, Mar. 1998.
- [69] Y. Sun, S. E. Thompson, and T. Nishida, "Physics of strain effects in semiconductors and metal-oxide-semiconductor field-effect transistors," *J. Appl. Phys.*, vol. 101, no. 10, pp. 1–22, 2007.
- [70] P. B. Sorokin, A. G. Kvashnin, D. G. Kvashnin, J. A. Filicheva, P. V Avramov, A. S. Fedorov, and L. A. Chernozatonskii, "Theoretical Study of Atomic Structure Nanowires," vol. 4, no. 5, pp. 2784–2790.
- [71] K. Yashiro and M. Fujihara, "Molecular dynamics study on atomic elastic stiffness in Si under tension: homogenization by external loading and its limit," *Model. Simul. Mater. Sci. Eng.*, vol. 20, no. 4, p. 045002, Jun. 2012.
- [72] C. Y. Tang, L. C. Zhang, and K. Mylvaganam, "The mechanical properties of a silicon nanowire under uniaxial tension and compression 1 Introduction 2 Modelling," no. December, 2007.
- [73] K. Yamamoto, H. Ishii, N. Kobayashi, and K. Hirose, "Effects of Vacancy Defects on Thermal Conduction of Silicon Nanowire: Nonequilibrium Green's Function Approach," *Appl. Phys. Express*, vol. 4, no. 8, p. 085001, Jul. 2011.
- [74] C. Abs da Cruz, K. Termentzidis, P. Chantrenne, and X. Kleber, "Molecular dynamics simulations for the prediction of thermal conductivity of bulk silicon and silicon nanowires: Influence of interatomic potentials and boundary conditions," *J. Appl. Phys.*, vol. 110, no. 3, p. 034309, 2011.
- [75] F. Fortuna, V. a. Borodin, M.-O. Ruault, E. Oliviero, and M. a. Kirk, "Synergetic effects

- of dual-beam implantation on the microstructural development in silicon,” *Phys. Rev. B*, vol. 84, no. 14, p. 144118, Oct. 2011.
- [76] D. Yao, G. Zhang, G.-Q. Lo, and B. Li, “Impacts of size and cross-sectional shape on surface lattice constant and electron effective mass of silicon nanowires,” *Appl. Phys. Lett.*, vol. 94, no. 11, p. 113113, 2009.
- [77] A. Henriksson, G. Friedbacher, and H. Hoffmann, “Surface modification of silicon nanowires via copper-free click chemistry,” *Langmuir*, vol. 27, no. 12, pp. 7345–8, Jun. 2011.
- [78] S. Kim, M. Jo, S. Jung, H. Choi, J. Lee, M. Chang, C. Cho, and H. Hwang, “Improvement of interface quality by post-annealing on silicon nanowire MOSFET devices with multi-wire channels,” *Microelectron. Eng.*, vol. 88, no. 3, pp. 273–275, Mar. 2011.
- [79] T. Tezuka, E. Toyoda, S. Nakaharai, T. Irisawa, N. Hirashita, Y. Moriyama, N. Sugiyama, N. Taoka, Y. Yamashita, M. Harada, T. Yamamoto, and S. Takagi, “Observation of Mobility Enhancement in Strained Si and SiGe Tri-Gate MOSFETs with Multi-Nanowire Channels Trimmed by Hydrogen Thermal Etching Mobility Characterization,” pp. 6–9, 2007.